Chemical Engineering Science 101 (2013) 374–381

Contents lists available at SciVerse ScienceDirect

Chemical Engineering Science

journal homepage: www.elsevier.com/locate/ces

Effect of hydrothermal treatment on Cr-SiO_2 mesoporous materials

Pablo M. Cuesta Zapata [a], Marcelo S. Nazzarro [d], Mónica L. Parentis [b], Elio E. Gonzo [b], Norberto A. Bonini [c,*]

[a] INIQUI–CONICET–CIUNSa–Fac. de Ciencias Exactas, Argentina
[b] INIQUI—CIUNSa—Fac. de Ingeniería, Argentina
[c] INIQUI–CIUNSa–Fac. de Ciencias Exactas, Avda. Bolivia 5150, 4400 Salta, Argentina
[d] INFAP—CONICET—Departamento de Física, Avda. Ejército de los Andes 950, 5700 San Luis, Argentina

HIGHLIGHTS

- Sol–gel followed by hydrothermal treatment let to obtain MCM-41 Cr/SiO_2 materials.
- The Cr^{+3} ions are stable and resistant to segregation in air up to 300 °C.
- The Cr^{+3} ions produce Lewis acid sites that catalyze the 2-propanol dehydration.
- XPS determine the dispersion and the Cr^{+3}/Cr^{+6} ratio on the synthesized materials.

GRAPHICAL ABSTRACT

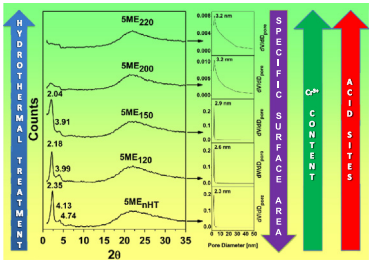

ARTICLE INFO

Article history:
Received 28 February 2013
Received in revised form
21 June 2013
Accepted 24 June 2013
Available online 8 July 2013

Keywords:
Nanostructure
Catalysis
Gels
Surfactant
Cr/MCM-41
Sol–gel

ABSTRACT

Cr/SiO_2 (MCM-41) materials were prepared by the sol–gel method by hydrolysis of tetraethylortosilicate (TEOS) using cetyltrimethylammonium bromide (CTAB) as a template. The effect of hydrothermal treatment between 120–220 °C on the structural properties was studied. Well ordered Cr/MCM-41 with a very narrow pore size distribution was obtained after hydrothermal treatment from RT to 150 °C.

Materials synthesized at higher temperatures (200 or 220 °C) showed the collapse of the ordered mesoestructure to give mesoporous Cr/SiO_2 with an open surface. Superficial Cr^{3+}/Cr^{6+} ratio was determined by XPS over materials hydrothermically synthesized at different temperatures, and calcined in air at 300 °C. The hydrothermal treatment improved the chromium to silica interaction, promoting a higher resistance to form Chromium (VI) sites. The chromium (III) ions incorporated to the silica structure developed acid sites responsible for the 2-PrOH dehydration.

1. Introduction

Chromium/SiO_2 catalysts are used in many industrial processes such as: polymerization of ethylene (Demmelmaier et al., 2009; Groppo et al., 2005; McDaniel, 2010; Weckhuysen et al., 1996; Zecchina et al., 2005), dehydrogenation and oxidative dehydrogenation of linear hydrocarbons (Martyanov and Sayari, 2008; Rao et al., 2009; Santamaría-González et al., 2000), cycloalkanes (Sakthivel and Selvam, 2002; Shylesh et al., 2007; Subrahmanyam et al., 2003), or benzyl (Mohapatra and Selvam, 2007; Shaikh et al., 2008) compounds. They are also used in water gas shift reaction (Jóźwiak et al., 2004).

A great number of studies were performed to determine the amount and the nature of the chromium species formed on the surface of these catalysts and to characterize the chemical structure of the active sites responsible for the catalytic behavior. The more extended characterization studies were carried out over

* Corresponding author. Tel.: +54 387 4255363; fax: +54 387 4255006.
E-mail addresses: pcuesta@unsa.edu.ar (P.M. Cuesta Zapata), nazzarro@unsl.edu.ar (M.S. Nazzarro), mparentis@unsa.edu.ar (M.L. Parentis), gonzo@unsa.edu.ar (E.E. Gonzo), bonini@exa.unsa.edu.ar (N.A. Bonini).

0009-2509/$ - see front matter © 2013 Elsevier Ltd. All rights reserved.
http://dx.doi.org/10.1016/j.ces.2013.06.041

the Cr/SiO_2 Phillips catalyst, which is responsible for more than one-third of all the polyethylene (PE) produced in the world (Groppo et al., 2005; McDaniel, 2010; Zecchina et al., 2005). Despite these efforts, some aspects of the active sites remain controversial, both for the multiplicity of the oxidation states of chromium, but also for the complex structure of the amorphous silica support. The more active catalysts were those obtained by CrO_3 impregnation (1% aprox.), calcined in air at or above 450 °C to develop a material with approximately two isolated-chromate ions per nm^2 (Santamaría-González, J., 2000). In these catalysts, the polymerization active sites were Cr^{+2} ions anchored to silica surface following CO or ethylene reduction of the chromate species precursors. Under these conditions, three different Cr^{+2} coordinatively unsaturated species were reported: Cr^{II}_A, Cr^{II}_B, and Cr^{II}_C. They were characterized by CO and/or NO adsorption. These Cr^{+2} ions are attached to the silica surface by Si–O–Cr bonds with an increasing number of oxygen ligands. They are forming chromasiloxane rings whose strain increases parallel to the decrease of the amount of atoms forming the cycles. Recently, Demmelmaier et al.(2009) reported that the six members strained rings, more abundant on catalyst pretreated at higher temperatures, develop higher ethylene polymerization activities probably because of their higher insaturation.

It is well known that the anchoring process of Cr^{6+} or Cr^{3+} ions happens through an esterification reaction, where the silica surface hydroxyl groups are consumed as chromium is attached to the surface by oxygen linkages (Groppo et al., 2005). Hexavalent chromium catalysts are obtained after thermal activation in temperatures up to 450 °C. Alternatively, Cr(III) catalysts were prepared by ion exchange methods (Paréntis, 2002). In this case, both mononuclear and binuclear Cr^{+3} ammoniacal complexes were exchanged on Si–OH groups to obtain grafted Cr^{+3} unsaturated ions. These catalysts were active for alcohol dehydrogenation and oxidehydrogenation in the gas phase. A moderate acidity (Brönsted and Lewis) on these materials was determined by Pyridine adsorption after calcination in air up to 450 °C. The final chromium/silica interactions depend on several factors such as, textural properties of the support, chromium loading, and temperature and oxidant atmosphere of calcination.

According to bibliography (Takehira et al., 2004), only one type of chromates were formed over Cr–MCM-41 prepared under direct hydrothermal synthesis (DHT) at 423 K with the redox system Cr^{+3}(octahedral)/Cr^{+6}(tetrahedral) being involved in the oxidative dehydrogenation of propane. The same authors found this catalyst showed a high selectivity in the oxidation of CH_4 to HCHO (Wang et al., 2003).

In a recent paper (Cuesta Zapata et al., 2013) it was shown that Cr/SiO_2 catalysts obtained by the sol–gel method, combined with hydrothermal treatment between 120 °C and 220 °C, are materials where Cr^{3+} ions incorporate into the silica structure through the formation of $SiO–Cr^{3+}$ bonds, going from a tetrahedral environment to a distorted octahedral one. These Cr^{3+} ions are incorporated through chromasiloxane rings developing Lewis acid sites whose strength increases as calcination temperature in air increases up to 350 °C. These sites, highly unsaturated, were responsible for the 2-propanol (2PrOH) dehydration. A fraction of these sites oxidized to Cr^{6+} when materials were heated in air or oxygen, producing weak Brönsted acid sites. Both, Lewis and Brönsted acid sites were identified through the adsorption of 2–6 Lutidine. The amount of Cr^{6+} formed depends on the temperature of the hydrothermal treatment. These sites were able to produce a reversible Cr^{3+}/Cr^{6+} system. The resistance to segregation of Cr^{6+} ions depends on chromium loading, hydrothermal treatment temperature, calcinations temperature, and oxidant conditions.

From the previous findings, it was demonstrated that Cr^{3+} ions anchored and incorporated to the SiO_2 structure by chromium siloxane bonds (Demmelmaier et al., 2009; Groppo et al., 2005) are important precursors in the reversible redox system involved in the reactions in which these catalysts are applied. Accordingly, the sol–gel method, followed by a hydrothermal treatment at different temperatures (120–220 °C), is a good alternative to control this chromium/silica interaction.

The present study shows a successful incorporation of chromium into the tetrahedral lattice of well ordered and mesostructurated MCM-41 silica through the synthesis of the gel in presence of cetyltrimethylammonium bromide as template and subsequent hydrothermal treatment (120–220 °C). The hydrothermal treatment followed by a controlled calcination to remove the surfactant allows modulating the interaction and control the Cr^{+3} environments. Consequently, synthesis, characterization, and catalytic activity of mesoporous (MCM-41) Cr/SiO_2 materials obtained by the sol–gel method combined with a hydrothermal treatment, between 120 and 220 °C, are reported.

2. Experimental

2.1. Sample preparation

2.1.1. Reactants

Reactants used to synthesize the samples were tetraethylorthosilicate (TEOS) (Merck $>98\%$) as silica source; cetyltrimethylammonium bromide (CTAB) (Fluka) as surfactant; $Cr(NO_3)_3.9H_2O$ (Anedra $>98\%$) as chromium source; tetramethylammonium hydroxide (TMAOH) (Merck—20% aqueous solution); ethanol (EtOH) (Merck—99,9%); and distilled water.

2.1.2. Procedure

15 g of CTAB dissolved in 137 mL of water were added to a mixture of 38 mL of TEOS, 137 mL of distilled water, and 180 mL of EtOH under vigorous stirring for 30 min at room temperature (RT). After that, 4.1 g of $Cr(NO_3)_3.9H_2O$ dissolved in 100 ml of H_2O:EtOH (1/1) solution was slowly added to the mixture, which was stirred for 90 min. The solution was heated up to 50 °C and 20 mL of TMAOH 25% was then added. The molar composition of the mixture was $1.0TEOS:0.24CTAB:105H_2O:25ETOH:0.25TMAOH:0.06Cr$. The mixture was allowed to gel during 24 h. Portions of the gel were placed in a Teflon vessel and autoclaved at different temperatures between 120 and 220 °C (hydrotreatment) in a H_2O:EtOH media. After the hydrothermal treatment, the solid product was filtered and washed with water and EtOH/acetone (1:1) mixture to remove the non-reacted chromium. The obtained solid was dried at 110 °C, calcined in a nitrogen flow at 550 °C for 19 h and finally treated in an air flow at 300 °C for 3 h to remove the surfactant. The presence of surfactant was monitored by FTIR spectroscopy. The materials were assigned as $5ME_{xxx}$ where xxx is the temperature of hydrotreatment.

2.2. Sample characterization

2.2.1. Textural characterization

Adsorption–desorption isotherms were carried out in a Micromeritics ASAP-2020 sorptometer, employing N_2 as the adsorbent. Specific surface area was calculated using the standard BET method on the basis of adsorption data in a relative pressure range from 0.05–0.35. The pore size distributions were calculated from the adsorption branches of the isotherms using the BJH method.

2.2.2. X-ray diffraction (DRX)

Crystallography studies and the mesoporous array of the samples were carried out in a RIGAKU-DENKI D-Max IIC powder diffractometer with a Cu-Kα emission of 40 V.

2.2.3. Fourier transform infrared spectroscopy (FTIR)

The FTIR spectra were recorded on a Spectrum GX-FTIR Perkin-Elmer spectrophotometer. Transmission spectra were obtained from the samples diluted with KBr and pressed at 2 Tn/cm^2. The spectra were determined in the 4000–350 cm^{-1} spectral range. All the spectra were normalized to the height of the SiO_4 band at the 1150–1000 cm^{-1} region.

2.2.4. UV–vis diffuse reflectance spectroscopy (DRUV–vis)

Analysis was carried out in a GBC-918 equipment with a diffuse reflectance sphere and $BaSO_4$ as the reference. Spectra in the 190–900 nm spectral range were determined from previously grounded and hand pressed samples.

2.2.5. X-ray photoelectron spectroscopy (XPS)

X-ray photoelectron spectroscopy (XPS) was performed in situ using a VG Microtech ESCA spectrometer with a non-monochromatic Al Kα radiation (300 W, 15 kV, $h\nu = 1486.6$ eV) as the excitation source combined with a VG-100-AX hemispherical analyzer operating at 25 eV pass energy. The instrumental resolution was 0.1 eV. The Si2p peak at 103.4 eV was taken as the reference for the binding energy (BE) calibration. Samples were outgassed at room temperature in the preparation chamber (10^{-6} Torr), until constant pressure was achieved and then introduced to the analysis chamber (10^{-9} Torr) for recording the spectra.

2.2.6. Atomic absorption spectroscopy (AAS)

Chromium loading was determined by Atomic Absorption Spectroscopy (AAS) with a GBC 904 AA Spectrometer after dissolving the samples with HF.

2.3. Determination of the surface acidity

The catalytic activity against 2-propanol (2-PrOH) was determined at atmospheric pressure in a Pyrex tubular, gas flow reactor (internal diameter = 5 mm). The catalyst amount varied from 50 to 100 mg (80–100 mesh). N_2 was used as carrier gas at a flow rate of 180 ml/min. 2-PrOH was vaporized in the carrier gas to obtain a partial pressure of 0.05 atm. The composition of the effluents was determined by a gas chromatograph equipped with a combined column of Haye-Sept and Chromosob 102, and a thermal conductivity detector. Experiments varying both the flow rate and the amount of catalyst were carried out in order to ensure the absence of diffusion control effects. The reaction rates were calculated from conversion values obtained after the steady state was reached at the desired temperature. These values were obtained in the increasing temperature step (up to 320 °C) as well as in the decreasing temperature step (down to 250 °C). The apparent activation energies (Ea) were determined from the $\ln r$ vs. $1/T$ plots, previously adjusted by the minimum square statistical method ($R^2 > 0.98$), in the 250–320 °C temperature range.

3. Results and discussion

3.1. X-ray diffraction (XRD)

Fig. 1 shows the XRD patterns of the synthesized materials as a function of the hydrothermal treatment. The XRD pattern of the sample without hydrothermal treatment ($5ME_{nHT}$) shows the characteristic reflection lines of a MCM-41 type material. This material develops peaks at 2.35, 4.13, and 4.74 units of 2θ (theta), and a weak peak at 6.24 units (Fig. 1). These signals were assigned to the (hkl) reflections of (1 0 0), (1 1 0), (2 0 0) and (2 1 0) planes respectively, and indexed as a 2-D hexagonal p6mm symmetry

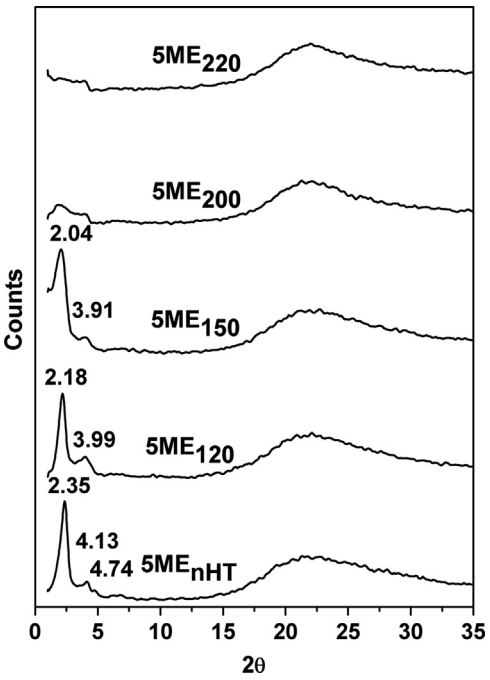

Fig. 1. XRD of mesoestructurated samples after different hydrothermal treatments.

resembling a highly ordered hexagonal structure (Barton et al., 1999; Kresge et al., 1992). As the hydrotreatment temperature increased to 150 °C, the intensity of the peaks decreased, with a little broadening. In the XRD diffractogram of the sample treated at 150 °C ($5ME_{150}$), the (2 0 0) signal almost disappeared, while the (2 1 0) plane is missing (Fig. 1). These changes are associated with a shift of the (1 0 0) reflection to a lower 2θ value. Accordingly, this diffraction line shifts from a 2θ value of 2.35 for ME_{nHT}, to 2.04 for ME_{150}, resembling the change in the cell parameter a_0, from 4.0 to 5.0 nm. The a_0 value depends on the pore size (Dp) and the wall thickness (t) ($a_0 = Dp + t$) (Mokaya et al., 2000). However, in the XRD of samples treated above 150 °C (Fig. 1), these lines almost disappear, showing a total collapse of the ordered mesoporous structure of the catalyst synthesized at 220 °C.

Besides the previously described peaks, a broad band centered between $2\theta \approx 21$–23, characteristic of amorphous silica which constitutes the walls of this type of mesoporous materials is observed. As hydrotreatment temperature increases up to 220 °C, an incipient diffraction line at $2\theta = 22.1$ develops, owing to the reorganization of the support for a more ordered siliceous matrix. At higher values of 2θ, notwithstanding the hydrothermal treatment, peaks assignable to the crystalline structures of chromium oxides were absent on the different Cr/SiO_2 materials.

3.2. N_2 adsorption isotherms

Low-temperature N_2 adsorption–desorption isotherms allow the measurement of specific surface area, pore volume and pore size distribution. Fig. 2 shows the N_2 adsorption–desorption isotherms on ME_{nHT}, ME_{120} and ME_{150} materials. They exhibited Type IV isotherms, characteristic of mesoporous solids in agreement with the IUPAC classification (Sing, 1985). In addition, ME_{120} and ME_{150} show a hysteresis loop (type H4), characteristic of solids with inter-particle pores (Sing, 1985).

The strong V_{N2} variation observed at low pressures ($p/p_0 < 0.1$) is due to monolayer-multilayer adsorption of N_2 on the walls of the mesopores. At P/P_0 values of between 0.2 and 0.4, isotherms exhibit an inflection resembling capillary condensation inside the primary mesopores. Nevertheless, N_2 adsorption–desorption

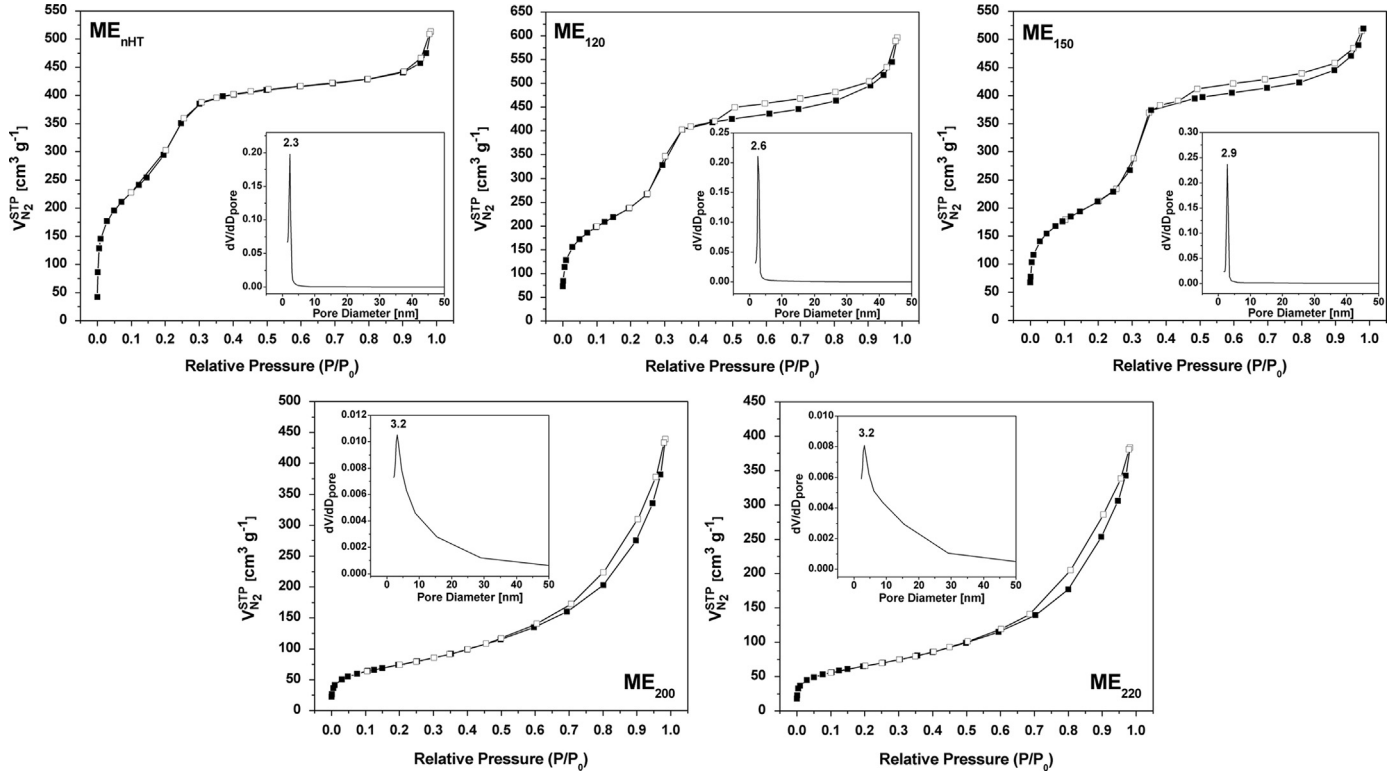

Fig. 2. N_2 Adsorption–desorption isotherms and pore size distribution.

Table 1
Textural properties of prepared materials.

Sample	BET surface area ($m^2\,g^{-1}$)	Pore volume ($cm^3\,g^{-1}$)	Pore diameter (nm)
5ME	1344	0.779	2.3
$5ME_{120}$	870	0.884	2.6
$5ME_{150}$	776	0.796	2.9
$5ME_{200}$	267	0.652	3.2
$5ME_{220}$	237	0.579	3.2

isotherms for ME_{200} and ME_{220} (Fig. 2) exhibited Type II isotherms distinctive of solids with open surface (Sing, 1985). The H3 type hysteresis loop is typical of materials formed by aggregation of particles (Sing, 1985).

Table 1 summarizes the textural properties of the 5ME materials after different hydrotreatments. As a trend, a decrease of the S_{BET} as the temperature of the hydrothermal treatment increased was observed (Fig. 3). Material without hydrotreatment ($5ME_{nHT}$) presented a S_{BET} value of 1344 m^2/g and a very narrow pore size distribution centered at 2.3 nm.

This value is usual in the MCM-41 mesoporous materials (Wang et al., 2003). In $5ME_{120}$ and $5ME_{150}$ materials a decrease of the S_{BET}, to a value of 776 $m^2\,g^{-1}$ in the sample treated at up to 150 °C, was observed. Both showed unimodal pore size distribution, characterized by an intense sharp peak centered at 2.6 and 2.9 nm, respectively. Therefore, and taking into account that the a_o parameter depends on Dp and t, it can be concluded that the decrease in the S_{BET} value is as a consequence both of the pore collapse and the wall thickness increase.

Conversely, in materials synthesized at higher temperatures (ME_{200} and ME_{220}), the decrease of the S_{BET} is more important (80% and 82% respectively). In these cases, they show a peak with a maximum at 3.2 nm overlapped to a broad one that resembles a pore size distribution characteristic of amorphous silica without

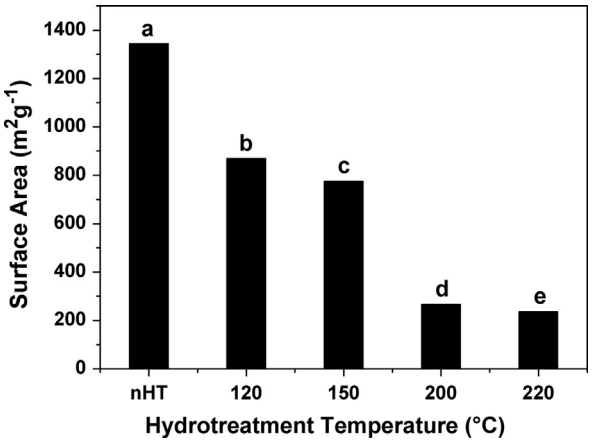

Fig. 3. Variation of S_{BET} as a function of hydrotreatment temperature (°C): (a) $5ME_{nHT}$, (b) $5ME_{120}$, (c) $5ME_{150}$, (d) $5ME_{200}$ and (e) $5ME_{220}$.

an ordered porous structure. This behavior is due to the destruction of the ordered mesoporous MCM-41 structure in agreement with that observed by XRD.

3.3. Infrared spectroscopy (FTIR)

Fig. 4 shows the FTIR spectra, in the range of 1350–450 cm^{-1}, of the KBr diluted waffers of catalysts synthesized at different hydrotreatment temperatures. All the materials develop bands at 470, 805, 966 and 1100 cm^{-1}; the last band with a shoulder at 1200–1220 cm^{-1}. The band at 470 cm^{-1} is assigned to the ρ(Si-O-Si) bending mode, while the bands centered at 805 cm^{-1}, together with the broad band with a shoulder at 1100 cm^{-1}, correspond to the symmetric ν_s(Si-O-Si) and asymmetric ν_{as}(Si-O-Si) stretching modes of the SiO_4 tetrahedral silica structure.

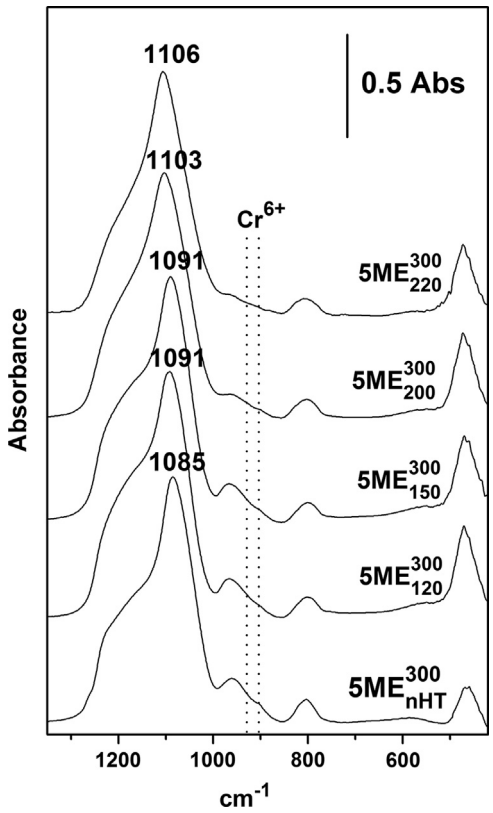

Fig. 4. FTIR spectra of 5ME; variation as a function of hydrothermal treatment.

The width of the band at 1100 cm^{-1}, and its location at frequencies lower than 1100 cm^{-1}, reflects the heterogeneity of the Si-O-Si bonds characteristic of an amorphous structure composed by different Q_n olygomeric species; where $n=0$–4 is the number of next-nearest neighboring Si atoms. It was demonstrated (Zholobenko et al., 1997) that Q_3 olygomers (ν_{as} 1040–1060 cm^{-1}) are the more abundant in the MCM-41 wet materials but they decrease after drying and/or calcination as a result of further condensation forming Q_4 olygomeric units ($\nu_{as}=1100$–1120 cm^{-1}). The narrowing of this band and the shift with the hydrothermal treatment from 1085 cm^{-1} to 1105 cm^{-1} (Fig. 4) reflects this behavior. The evolution of the shoulder at 1200–1220 cm^{-1} shows the almost total disappearance of the Q_3 units (1220 cm^{-1}) to form Q_4 olygomers (1180 cm^{-1}) producing a typical amorphous SiO_2 material composed mainly by Q_4 units. This behavior is in agreement with that previously observed by XRD (Fig. 1).

The 900–1000 cm^{-1} region shows the bands related to the stretching of Si-OH and Si-OM bonds, where M is a metal. The last signal is generally weak and difficult to detect at low metal concentration. Accordingly, the band at 970 cm^{-1} has been assigned to the Si-O bond vibration of the superficial hydroxyl groups. On the materials with a mesoporous ordered structure the Si-OH stretching band is centered at 975 cm^{-1}, and it decreases in intensity with hydrothermal treatment (Fig. 4). The decrease in the intensity of this band, when the temperature of hydrothermal treatment increases, can be related both to the formation of Si-OCr bonds and to the drop of the S_{BET} (Table 1).

Besides, the bands associated to the symmetric and antisymmetric stretching vibration of the O=Cr=O bonds in Cr^{6+} oxides appear in this region. So, the development of two bands at 905 and 955 cm^{-1} reveals their presence (Paréntis, 2002) (see dotted lines in the Fig. 4). Only the sample without hydrothermal treatment showed an incipient band at 905 cm^{-1}. The 955 cm^{-1} band probably overlaps with the Si-OH and Si-OCr stretching bands at 975–960 cm^{-1}.

3.4. X-ray photoelectron spectroscopy (XPS)

As has been reported, in supported Cr/SiO_2 materials chromium ions exist in different oxidation states, which are responsible of their catalytic behavior. In particular, Cr^{6+} and Cr^{3+} play an important role in the oxidation processes. Their relative amount is the key to determine their behavior in a reversible redox process, and in elucidating the nature of the active sites. XPS is a useful technique to determine their relative surface concentration (Liu and Terano, 2001; Rahman et al., 1995; Wagner, 1978; Zhang et al., 2008).

Fig. 5 illustrates the Cr_{2p} XPS spectra of the different ME's samples. To determine the Cr^{3+}/Cr^{6+} ratio, the spectra were deconvoluted using Lorentzian–Gaussian functions in order to fit them with the experimental spectra in the 595–570 eV range of BE. Deconvolution was done taking into account the BE and FWHM values for the Cr_{2p} signals obtained over Cr/SiO_2 catalysts reported in the bibliography (Liu and Terano, 2001; Rahman et al., 1995; Wagner, 1978; Zhang et al., 2008). However, getting a good fit using a single function to represent only Cr^{3+} or Cr^{6+} ions was not possible. This behavior shows the simultaneous presence of both ions. It was concluded that a fraction of the Cr^{3+} ions was oxidized to Cr^{6+} during the air calcination step (3 h at 300 °C); performed in order to remove the template (see Section 2).

According to data reported in the bibliography, Cr_{2p} signals centered at BE=577 and 586 eV must be assigned to Cr^{3+} ions, whereas Cr^{6+} ions develop signals centered at 579 and 588 eV. Table 2 lists the BE values and the width (FWHM) of the Cr_{2p} (3/2) bands observed on the samples.

The sample without hydrothermal treatment ($5ME_{nHT}$) shows signals that fit with chromium in two oxidation states. The first one, centered at 578.0 eV (FWHM=2.7 eV), was assigned to the presence of Cr^{6+} ions (52% of area); the second, at BE of 576.5 eV (FWHM=2.2), was assigned to Cr^{3+} (48% of area). Therefore, more than half of the surface chromium was oxidized when the sample was calcined in air for 3 hours at 300 °C. As the temperature of the hydrothermal treatment increased, a shift of both signals to higher values of BE was observed, leading to higher FWHM values.

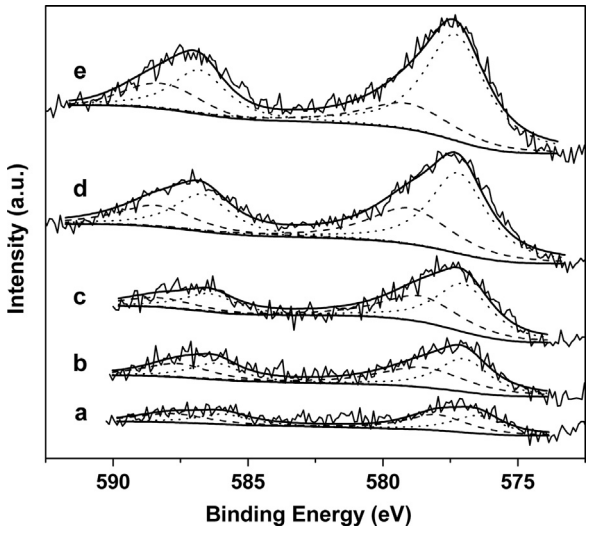

Fig. 5. Cr2p XPS spectra of materials treated at different temperatures. (a) $5ME_{nHT}$, (b) $5ME_{120}$, (c) $5ME_{150}$, (d) $5ME_{200}$ and (e) $5ME_{220}$.

Table 2
XPS parameters observed.

Sample	Cr 2p(3/2)		Oxidation state assignment	Atomic percentage (%)	Cr/Si	A_F (%)[a]	Total Cr content (%)[b]
	BE (eV)	FWHM (eV)					
5ME	576.5	2.2	3+	48	0.153	4.1	3.5
	578.0	2.7	6+	52			
$5ME_{120}$	577.0	2.3	3+	50	0.045	1.2	3.9
	578.5	3.8	6+	50			
$5ME_{150}$	577.0	2.4	3+	57	0.052	1.4	4.0
	578.6	3.4	6+	43			
$5ME_{200}$	577.2	2.5	3+	61	0.077	2.0	4.0
	579.0	3.6	6+	39			
$5ME_{220}$	577.2	2.7	3+	75	0.083	2.3	4.0
	579.0	3.8	6+	25			

[a] (% atomic fraction) Determined by XPS from the areas of O 1s, Si 2p and Cr 2p signals [24].
[b] (*w*/*w*) Determined by Atomic Absorption Spectroscopy.

The BE of the Cr2p levels shifts to higher values both with increasing chromium oxidation state and for a certain oxidation state, with increasing the electronegativity of the surrounding atoms. For these reasons, on Cr/SiO_2 catalysts with chromium in a fixed oxidation state, the shift in the BE is directly related to an increase in the metal-support interaction by the formation of Cr–OSi bonds (Liu and Terano, 2001). Moreover, the shift of BE to higher values can be strengthened by increasing strain in the surface siloxane groups where chromium ions are fixed. The observed shift in BE (Table 2) reveals how the interaction with the support improved as the hydrotreatment temperature increased. While the $5ME_{nht}{}^{300}$ the BE of Cr^{+3} signal appeared at 576.5 eV, it shifted to 577.2 eV as the hydrotreatment temperature rose to 220 °C. The last BE value was assigned to surface-stabilized trivalent Cr(III) ions on SiO_2 (Liu and Terano, 2001). Consequently, a higher Cr^{3+}/Cr^{6+} atomic ratio was observed for samples synthesized at higher temperatures, providing a greater resistance to oxidation. The shift of 1 eV observed for the Cr^{+6} signal indicates that in $5ME_{220}{}^{300}$, these oxidized species are fixed to the silica surface forming a monochromate structure. On the other hand, the increase of the FWHM value reflects the existence of different chromium species in a given oxidation state, probably with different coordination and/or unsaturation degree.

Atomic fraction (A_F) of chromium, determined from the relative intensity of the XPS signals corresponding to Cr, O and Si, represents the amount of chromium exposed on the surface. Fig. 6 shows the evolution of A_F as the temperature of the hydrothermal treatment changed. The sample without hydrotreatment shows the greater amount of chromium exposed, proving that during gelification chromium (III) reacts with small oligomers of silica ("sols") covered with external Si-OH groups (Brinker, 1990). By contrast, hydrothermal treatment up to 150 °C causes both the redissolution of silica and Si-O-Cr bond formation, precipitating and causing the occlusion of a fraction of chromium. As temperature increased (200–220 °C), the mesoporous structure collapsed, the S_{BET} decreased and the amount of exposed chromium increased progressively (Fig. 6).

On the other hand, the low intensity of Cr_{2p} signal observed in materials without hydrotreatment (Fig. 5a) suggests that most of the chromium is on the inner surface, hidden into the pores and not detected for the XPS technique. It is known that XPS detection is limited by the mean photoelectron escape depth to about 2 nm. Consequently, high mesoporous materials only exhibit a very low surface to the XPS beam. As the severity of the hydrotreatment increases, and the mesoporous structure is gradually destroyed, the intensity of the signal increases as a result that the exposed surface, visible by XPS, is higher.

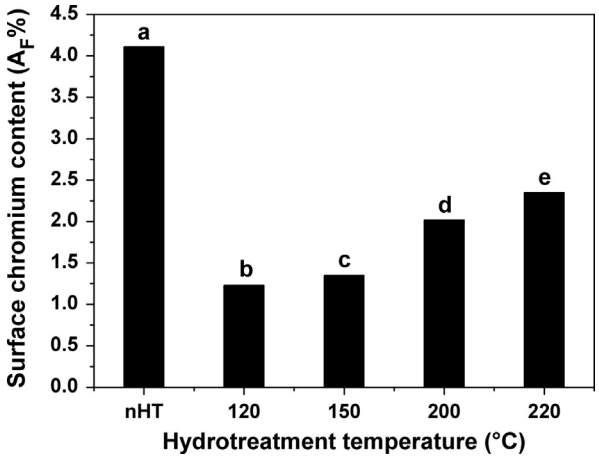

Fig. 6. Variations in surface chromium content (%) as a function of hydrotreatment temperatures: (a) $5ME_{nHT}$, (b) $5ME_{120}$, (c) $5ME_{150}$, (d) $5ME_{200}$ and (e) $5ME_{220}$.

3.5. Diffuse reflectance UV–vis spectroscopy (UV–vis DRS)

UV–vis DRS is a useful technique for analyzing Cr/SiO_2 catalysts. The color of the samples reflects the presence of the different species which appear on them. Green samples reveal the presence of Cr^{3+} ions; yellow or orange color is indicative of the Cr^{6+} species (chromate or polychromate); while a blue color is due to the presence of Cr^{2+}.

The Cr^{6+} ions (chromates and dichromates) supported on silica show four bands centered at 460, 350, 290 and 260 nm, approximately (Sakthivel et al., 2003; Weckhuysen et al., 1993). These bands are due to ligand-to-metal charge transfer transitions (LMCT). In the solid state, LMCT bands occur at higher wave numbers than those observed on similar compounds (chromate or dichromate) in liquid phase. The maxima (nm) of these bands depends on the chromate/dichromate ratio and, consequently, on their interaction with the silica surface (Puurunen et al., 2001; Sakthivel et al., 2003; Weckhuysen et al., 1993).

Nevertheless, Cr^{3+}/SiO_2 materials develop three intense bands centered at 640, 440 and 290 nm, approximately (Sakthivel et al., 2003). Therefore, while the 640 nm absorption band is indicative of the presence of Cr^{3+} ions, the development of a strong absorption at 350 nm (approximately) reveals the presence of the Cr^{6+} oxidized species.

Fig. 7 illustrates the UV–vis spectra of the samples. On the $5ME_{nHT}$ sample, absorption bands were detected at 260, 355, 447 and 665 nm. The first three bands are assigned to O→Cr(VI) LMCT

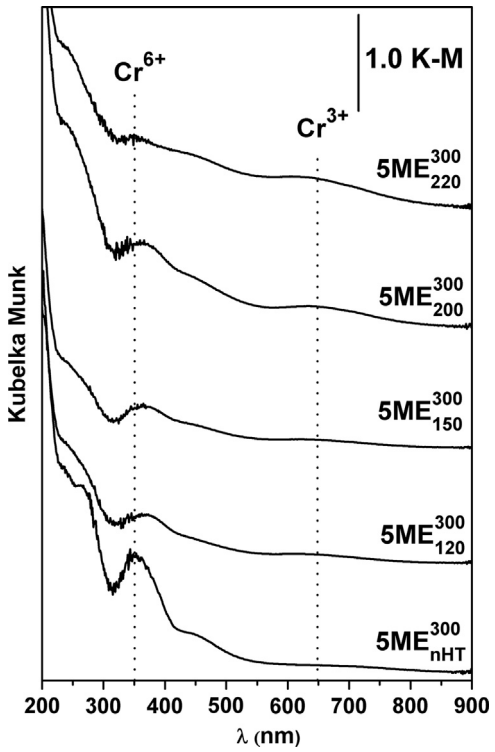

Fig. 7. DRUV–vis spectra of mesoestructurated samples as a function of hydrothermal treatment temperature.

bands of chromate-like species, with Cr^{6+} in tetrahedral coordination (Sakthivel et al., 2003; Weckhuysen et al., 1993). The weak band at 447 nm corresponds to a symmetry forbidden transition, while the two bands at 260 nm and 355 nm to symmetry allowed transitions. The band at 665 nm corresponds to the d–d transition $^4A_{2g}$–$^4T_{2g}$, characteristic of Cr(III) ion in a distorted octahedral coordination. In a previous paper (Cuesta Zapata et al., 2013) a shift of this bands from 610 to 645 cm^{-1}, with the hydrothermal treatment, was assigned to a progressive increase of the number of ligands through the Si-O-Cr bonds formation. The shift towards higher wavelengths was accompanied by a strong change in the relative intensities of the absorption bands at 645 and 460 cm^{-1} corresponding to the $^4T_{2g}$–$^4A_{2g}$ and $^4T_{1g}$–$^4A_{2g}$ d–d transitions respectively. These changes reflect the distortion of the octahedral field produced by the incorporation of Cr^{3+} ions into the tetrahedral structure of silica. This distortion was related to the formation of more strained chromium siloxane rings reported in the literature.

In conjunction with the increase of the hydrothermal treatment temperature, a decrease in the intensity of the band at 355 nm, corresponding to tetrahedral Cr^{6+}, and a concurrent increase of the signal at 665 nm due to Cr^{3+} ions was observed,. From this trend it is evident that the effect of hydrotreatment is to provide a higher resistance to oxidation as a consequence of the increased Cr–SiO_2 interaction observed by XPS.

3.6. Determination of surface acidity

In order to correlate the structural changes observed in the surface properties, a study of the catalytic activity of these catalysts against 2-propanol (2-PrOH) was conducted. This alcohol molecule allows evaluating the acid–basic properties of a solid, analyzing its capacity to produce different products. So, the formation of propene and/or isopropyl ether allows inferring the presence of acids centers, while 2-propanone allows inferring the simultaneous presence of basic and acid sites. Consequently and in accordance with bibliography (Gervasini and Auroux, 1991), amorphous SiO_2 and Cr_2O_3 show no dehydration activity in the 140–280 °C temperature range.

Table 3
Catalytic activity of the samples against 2-PrOH.

Sample	$r_{270\ °C}$ (mol ene s^{-1} m^{-2})	Selectivity (%)	Ea (Kcal/mol)
$5ME_{nHT}$	4.72 10^{-5}	79	22.7
$5ME_{150}$	2.23 10^{-4}	87	22.3
$5ME_{220}$	3.27 10^{-4}	91	20.5

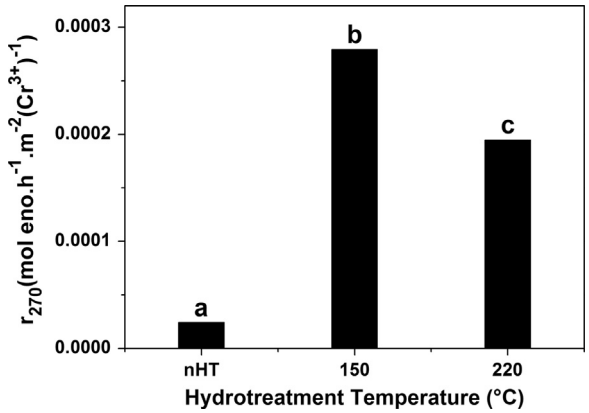

Fig. 8. Reaction rate of 2-propanol to propene at 270 °C, for different materials. (a) $5ME_{nHT}$, (b) $5ME_{150}$ and (c) $5ME_{220}$. (Cr^{3+}=A_F *x*% Cr^{3+} from XPS results).

Catalytic activity in the 2-propanol reaction showed that all the samples exhibit an acidic behavior evidenced by the high selectivity to the propene formation at 270 °C. The similar apparent activation Energy (Ea) observed among the different catalysts (Table 3) shows that changes in the reaction rate of the dehydration reaction are as a consequence of the variation in the amount of the acid sites, but not in the nature of the centers. However, the reaction rate (mol propene s^{-1} m^{2}) for the dehydration reaction was almost 10 times greater for the hydrothermally treated catalyst at 150 or 220 °C than for the materials without hydrotreatment. This behavior is evidenced in Fig. 8, where we represent the dehydration reaction rate (270 °C), divided by the atomic fraction of surface Cr^{3+} (A_F *x*%Cr^{3+}) determined by XPS (Table 2). In this figure we can observe that reaction rates for hydrothermally treated materials are one order of magnitude greater than for the materials prepared without hydrotreatment.

$5ME_{nHT}$ material shown the lower dehydrogenation rate, demonstrating that the Cr^{+3} ions were weakly grafted into the silica surface in agreement with the low BE value observed. As the hydrothermal treatment increases up to 150 °C, it produces the progressive incorporation of Cr^{3+} ions, developing highly unsaturated Lewis acid sites. According to bibliography (Demmelmaier et al., 2009), these chromium sites are incorporated to silica structure thorough chromasiloxane rings whose strain increases with the hydrothermal treatment. The degree of insaturation of Cr^{3+} on these sites and hence his acidity depends on the size of the cycle. These highly unsaturated sites are responsible for 2-propanol dehydration. As the temperature of hydrotreatment was increased up to 220 °C and the mesoporous structure disappeared, a fraction of Cr^{3+} ions sank into the silica framework forming highly coordinated and hence nonreactive sites.

Conversely, oxygenated Cr^{6+} ions promote the dehydrogenation of 2-propanol to acetone. This reaction, more complex than dehydration, needs the simultaneous presence of both basic and acid sites (Gervasini and Auroux, 1991). Accordingly, the selectivity to propene was higher on materials where Cr^{6+} was scarcely formed.

4. Conclusions

This study shows the effect of hydrothermal treatment at 120–220 °C, on the structural properties of MCM-41 chromium/silica materials. This technique allows obtaining well-ordered mesoestructurated materials with a very narrow pore size distribution, when the samples are hydrothermally treated at temperatures ranging from RT to 150 °C. Materials synthesized at higher temperatures (200 or 220 °C) show a collapse of the MCM-41 mesoestructure, to give mesoporous materials an open surface. The hydrothermal treatment improved the chromium to silica interaction, observed by XPS binding energies, thorough chromasiloxane rings formation, whose strain increases with the hydrothermal treatment. These anchored chromium (III) ions develops unsaturated Lewis acid sites responsible of the 2-PrOH dehydration. Accordingly, the hydrotreatment increases the resistance to form Chromium (VI) sites when materials are calcined in air up to 300 °C.

Acknowledgments

This work was performed under the auspices and the financial support of INIQUI-CONICET and CIUNSa. The authors thank collaboration of Laboratorio de Física Experimental—Universidad Nacional de San Luis.

References

Barton, T.J., Bull, L.M., Klemperer, W.G., Loy, D.A., McEnaney, B., Misono, M., Monson, P.A., Pez, G., Scherer, G.W., Vartuli, J.C., Yaghi, O.M., 1999. Tailored Porous Materials. Chem. Mater. 11, 2633–2656.

Brinker, J.S.G., 1990. Sol–Gel Science: the Physics and Chemistry of Sol–Gel Processing. Academic Press, Inc., San Diego.

Cuesta Zapata, P.M., Parentis, M.L., Gonzo, E.E., Bonini, N.A., 2013. Acid sites development on Cr3+/SiO2 catalysts obtained by the sol–gel method and hydrothermal treatment: Effect of calcination temperature. Appl. Catal. A Gen. 457, 26–33.

Demmelmaier, C.A., White, R.E., van Bokhoven, J.A., Scott, S.L., 2009. Evidence for a chromasiloxane ring size effect in Phillips (Cr/SiO2) polymerization catalysts. J. Catal. 262, 44–56.

Gervasini, A., Auroux, A., 1991. Acidity and basicity of metal oxide surfaces, II. Determination by catalytic decomposition of isopropanol. J. Catal. 131, 190–198.

Groppo, E., Lamberti, C., Bordiga, S., Spoto, G., Zecchina, A., 2005. The structure of active centers and the ethylene polymerization mechanism on the Cr/SiO_2 catalyst: a frontier for the characterization methods. Chem. Rev. 105, 115–184.

Jóźwiak, W.K., Ignaczak, W., Dominiak, D., Maniecki, T.P., 2004. Thermal stability of bulk and silica supported chromium trioxide. Appl. Catal. A Gen. 258, 33–45.

Kresge, C.T., Leonowicz, M.E., Roth, W.J., Vartuli, J.C., Beck, J.S., 1992. Ordered mesoporous molecular sieves synthesized by a liquid–crystal template mechanism. Nature 359, 710–712.

Liu, B., Terano, M., 2001. Investigation of the physico-chemical state and aggregation mechanism of surface Cr species on a Phillips CrOx/SiO2 catalyst by XPS and EPMA. J. Mol. Catal. A Chem. 172, 227–240.

Martyanov, I., Sayari, A., 2008. Sol–Gel assisted preparation of chromia–silica catalysts for non-oxidative dehydrogenation of propane. Catal. Lett. 126, 164–172.

McDaniel, M.P., 2010. Chapter 3—A Review of the Phillips supported chromium catalyst and its commercial use for ethylene polymerization. In: Bruce, C.G., Helmut, K. (Eds.), Adv. Catal. Academic Press, pp. 123–606.

Mohapatra, S.K., Selvam, P., 2007. A highly selective, heterogeneous route to enones from allylic and benzylic compounds over mesoporous CrMCM-41 molecular sieves. J. Catal. 249, 394–396.

Mokaya, R., Zhou, W., Jones, W., 2000. Restructuring of mesoporous silica: high quality large crystal MCM-41 a seeded recrystallisation route. J. Mater. Chem. 10, 1139–1145.

Paréntis, M.B., Norberto, Gonzo, Elio, 2002. Dehydrogenation and oxidative dehydrogenation of alcohols on silica supported chromium catalysts Latin. Am. Appl. Res. 32, 41–46.

Puurunen, R.L., Beheydt, B.G., Weckhuysen, B.M., 2001. Monitoring chromia/alumina catalysts in situ during propane dehydrogenation by optical fiber UV–visible diffuse reflectance spectroscopy. J. Catal. 204, 253–257.

Rahman, A., Mohamed, M.H., Ahmed, M., Aitani, A.M., 1995. Characterization of chromia/alumina catalysts by X-ray photoelectron spectroscopy, proton induced X-ray emission and thermogravimetric analysis. Appl. Catal. A Gen. 121, 203–216.

Rao, T.V.M., Yang, Y., Sayari, A., 2009. Ethane dehydrogenation over pore-expanded mesoporous silica supported chromium oxide: 1. Catalysts preparation and characterization. J. Mol. Catal. A Chem. 301, 152–158.

Sakthivel, A., Dapurkar, S.E., Selvam, P., 2003. Allylic oxidation of cyclohexene over chromium containing mesoporous molecular sieves. Appl. Catal. A Gen. 246, 283–293.

Sakthivel, A., Selvam, P., 2002. Mesoporous (Cr)MCM-41: a mild and efficient heterogeneous catalyst for selective oxidation of cyclohexane. J. Catal. 211, 134–143.

Santamaría-González, J., Mérida-Robles, J., Alcántara-Rodríguez, M., Maireles-Torres, P., Rodríguez-Castellón, E., Jiménez-López, A, 2000. Catalytic behaviour of chromium supported mesoporous MCM-41 silica in the oxidative dehydrogenation of propane. Catal. Lett. 64, 209–214.

Shaikh, R.A., Chandrasekar, G., Biswas, K., Choi, J.-S., Son, W.-J., Jeong, S.-Y., Ahn, W.-S., 2008. Tetralin oxidation over chromium-containing molecular sieve catalysts. Catal. Today 132, 52–57.

Shylesh, S., Samuel, P.P., Singh, A.P., 2007. Chromium-containing small pore mesoporous silicas: synthesis, characterization and catalytic behavior in the liquid phase oxidation of cyclohexane. Appl. Catal. A Gen. 318, 128–136.

Sing, K.S.W.E., Haul, D.H., Moscou, R.A.W., Pierotti, L., Rouquérol, R.A., Siemieniewska, T., J., 1985. Reporting physisorption data for gas/solid systems with special reference to the determination of surface area and porosity. Pure Appl. Chem. 57, 603–619.

Subrahmanyam, C., Louis, B., Rainone, F., Viswanathan, B., Renken, A., Varadarajan, T.K., 2003. Catalytic oxidation of toluene with molecular oxygen over Cr-substituted mesoporous materials. Appl. Catal. A Gen. 241, 205–215.

Takehira, K., Ohishi, Y., Shishido, T., Kawabata, T., Takaki, K., Zhang, Q., Wang, Y., 2004. Behavior of active sites on Cr–MCM-41 catalysts during the dehydrogenation of propane with CO2. J. Catal. 224, 404–416.

Wagner, C.R.W., Davis, L., Moulder, J., Muilenberg, G., 1978. Handbook of X-Ray Photoelectron Spectroscopy. Perkin Elmer Corporation, Minessota.

Wang, Y., Ohishi, Y., Shishido, T., Zhang, Q., Yang, W., Guo, Q., Wan, H., Takehira, K., 2003. Characterizations and catalytic properties of Cr–MCM-41 prepared by direct hydrothermal synthesis and template-ion exchange. J. Catal. 220, 347–357.

Weckhuysen, B.M., De Ridder, L.M., Schoonheydt, R.A., 1993. A quantitative diffuse reflectance spectroscopy study of supported chromium catalysts. J. Phys. Chem. 97, 4756–4763.

Weckhuysen, B.M., Wachs, I.E., Schoonheydt, R.A., 1996. Surface Chemistry and Spectroscopy of Chromium in Inorganic Oxides. Chem. Rev. 96, 3327–3350.

Zecchina, A., Groppo, E., Damin, A., Prestipino, C., 2005. Anatomy of catalytic centers in phillips ethylene polymerization catalyst. In: Copéret, C., Chaudret, B. (Eds.), Surface and Interfacial Organometallic Chemistry and Catalysis. Springer, Berlin Heidelberg, pp. 1–35.

Zhang, L., Zhao, Y., Dai, H., He, H., Au, C.T., 2008. A comparative investigation on the properties of Cr-SBA-15 and CrOx/SBA-15. Catal. Today 131, 42–54.

Zholobenko, V.L., Holmes, S.M., Cundy, C.S., Dwyer, J., 1997. Synthesis of MCM-41 materials: an in situ FTIR study. Microporous Mater. 11, 83–86.